HIGH ENTROPY ALLOYS GENERATED WITH LASER CLADDING

Paper LAM1302

M. Kuczyk, L. Kotte, J. Kaspar, M. Barbosa, S. Nowotny, M. Zimmermann, C. Leyens

Fraunhofer Institute for Materials and Beam Technology (IWS), Dresden

Abstract

In this contribution the manufacture of high entropy alloys (HEA) by laser cladding using multiple powders is demonstrated. In-situ alloying via laser powder cladding is particularly interesting because it has the potential to be a cost-effective alternative to the use of pre-alloyed powders or blends. The coating deposition was carried out using the coaxial cladding system COAXpowerline, developed by Fraunhofer IWS and a 4 kW diode laser (980±10 nm). The coatings were characterized in terms of chemical and microstructural homogeneity by the analysis of cross-sections using Vickers micro-hardness measurements and advanced scanning electron microscopy including X-ray spectroscopy (EDS) and electron backscatter diffraction (EBSD).

Upon the inherent high solidification rate during processing grain refinement could be observed. A significant reduction in element separation was achieved, thus reducing the need for homogenization annealing. By this approach, $Al_xCoCrFeNi$ coatings could be manufactured reliably, demonstrating high chemical and structural homogeneity without macroscopic segregations and only with minor amounts of impurities. In the $Al_xCoCrFeNi$ system, the lattice structure could be easily adjusted via the Al content. A transition from the solid-solution FCC phase to a multiphase BCC microstructure was observed for Al contents > 15 at%, which resulted in a hardness increase from 200 HV to 500 HV in the system. Laser cladding can be considered as a simple and cost-effective process for a single-step production of HEA based coatings or volumes.

Introduction

The material class of high entropy alloys is gaining much interest due to the manifold possibilities of tailorable properties that far surpass conventional alloys. Depending on the alloy system unique high-temperature properties, such as excellent strength, superior corrosion resistance, good ductility and fracture toughness are achievable [1–5]. HEAs are defined as alloys consisting of five or more elements, with typical concentrations of each element between 5 at.% and 35 at.%. Due to the unique alloy design, the contribution of the configurational entropy (ΔS_{conf}) in HEAs is much higher than in conventional alloys. This is the reason why the formation of intermetallic phases is supressed in this type of alloys and solid solution phases such as FCC and BCC can be easily obtained [1, 4]. HEAs are expected to be attractive new structural materials that complement conventional alloys such as Ni-based superalloys and stainless steels. However, the manufacturing route of reliable HEA coatings or volumes starting from pre-alloyed powder is still technologically challenging and costly in particular because of the high number of constituent elements (> 5) with sometimes vastly different melting points.

The aim of this study is the generation of $Al_xCoCrFeNi$ alloys with varying aluminium contents using laser cladding. The $Al_xCoCrFeNi$ system is based on the well-studied CoCrFeMnNi composition, the so-called Cantor alloy [6]. Depending on the Al content the alloy exhibits high strength, good corrosion resistance and high ductility [7–9]. At Al contents below 7 at.% the alloy displays a solid solution FCC microstructure. Higher Al contents result in a transition into a multiphase BCC microstructure. At Al contents above 22 at.% this HEA typically solidifies in a dendritic, interdendritic microstructure due to elemental segregation. A dendritic Al, Ni rich ordered B2 phase and an interdendritic Cr, Fe rich solid solution BCC phase can be observed as a result [10, 11]. This HEA belongs to a new generation of materials with a promising use in high temperature applications and thermal barrier coatings.

Hereafter it will be shown that for this new material group laser cladding is a very suitable manufacturing process. Laser cladding is already applied at high scale into several industrial branches with the purpose of coating, part refurbishment but also for the manufacturing of functional 3D components. The process is suitable for a broad spectrum of materials (e.g., Fe-, Ni-, Co-, or Ti-based alloys) [12–15]. By combining several powder feeders, a variation of the elemental composition within the microstructure manufactured is feasible and therefore excellent for the evolution of new HEA systems. Moreover the high cooling rates (10^3-10^5 Ks^{-1}) achieved during laser cladding are advantageous to a significant none equilibrium solute-trapping effect. This prevents component segregation and counteracts the limitations associated with low solubility [13, 18]. In this study Al_xCoCrFeNi samples will be manufactured and their phase composition in the as-built condition and after homogenization will be compared. The microstructure and elemental segregation of the samples will be analysed using scanning electron microscopy (SEM) including X-ray spectroscopy (EDS) and electron backscatter diffraction (EBSD), additionally Vickers hardness profiles will be measured.

Experimental Details

Two powders were used for the deposition of the gradient structures: one pre-alloyed and atomized CoCrFeNi powder with particle sizes between 45 and 90 µm (produced by Nanoval GmbH, Germany) and pure Al powder with particle sizes between 63 and 150 µm (produced by Ecka Granules, Austria). The laser cladding tests were carried out using the cladding nozzle COAXpowerline developed at the Fraunhofer IWS. This is a coaxial ring nozzle with powder focus diameter of 1.9 to 2.2 mm. The size of the powder focus diameter is determined by the powder feed rate and its carrier gas volume flow. Laser cladding took place in an Ar atmosphere at a working distance (distance between substrate and nozzle tip) of 13 mm. The argon atmosphere is generated in a shielding gas chamber, also developed by the Fraunhofer IWS, having a slight overpressure of 200 mbar at 20 ppm residual oxygen. A laser spot diameter of 3.81 mm is used for optimum powder utilization. The powder is introduced into the nozzle via four evenly distributed powder inlets. A powder distributor is connected in front of powder inlets, in which the two base powders are fed. With each cladding layer it is possible to change the powder composition and thus create gradient layers. A 4 kW diode laser from Laserline GmbH was used for the laser cladding process. The test assembly can be seen in Fig. 1. The gradient volume is composed of nine single layers which were welded unidirectionally. Stainless steel 1.4301 is used as substrate material. The powder feed rates of the two powders CoCrFeNi and Al were varied as described in Tab. 1. The total powder feed rate was kept constant at 20 g/min. All samples were welded with laser power of 1700 W and process velocity of 600 mm/min.

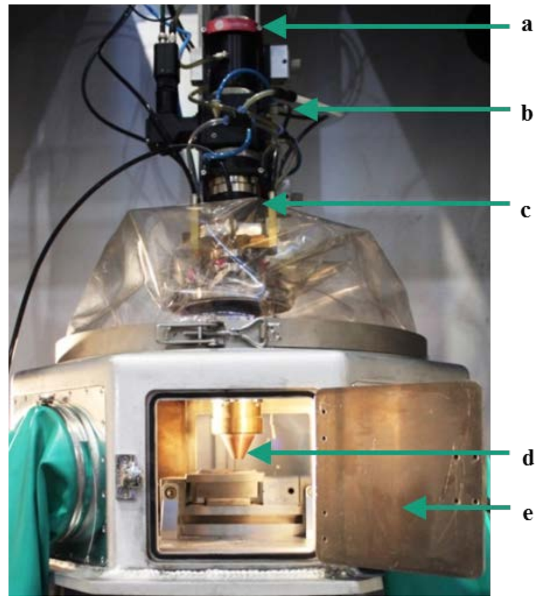

Fig. 1 Laser cladding test assembly: a) fiber plug; Laser LDM4000-100, Laserline GmbH; b) Powder inlets; c) OTS-2-optic with laser-focus of 3.8 mm; d) Powder-nozzle COAXpowerline with powder-focus of 1.9 – 2.2 mm; e) Shielding gas chamber with Ar (O_2 < 20 ppm)

For the microstructural investigations the samples were cut and mounted using a cold mounting epoxy resin. The samples were grinded with SiC abrasive paper, wet-polished using a diamond polishing suspension and finally vibratory polished for multiple hours using Al and Si oxide polishing suspensions. Microstructure investigation was carried out by scanning electron microscopy (SEM), energy

Tab. 1 Powder feed rate for gradient layers

layer	powder feed rate in g/min CoCrFeNi	Al	powder feed rate in g/min CoCrFeNi	Al	powder feed rate in g/min CoCrFeNi	Al
1. - 3.	19.5	0.5	19.5	0.5	19.0	1.0
4. - 6.	19.0	1.0	18.4	1.6	17.8	2.2
7. - 9.	18.4	1.5	17.3	2.7	16.6	3.4
system	**5/10/15**		**5/15/25**		**10/20/30**	

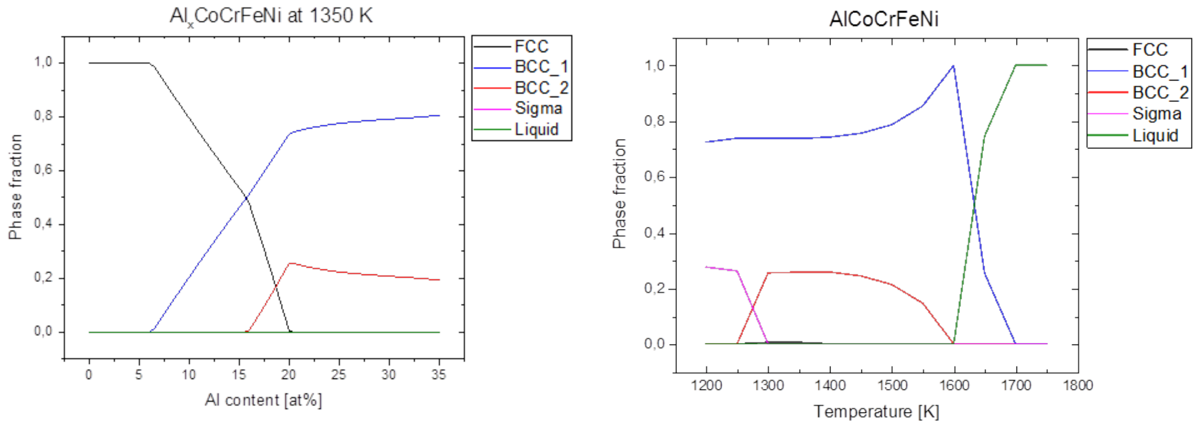

Fig. 2 CALPHAD simulation of expected phase composition at 1350 K for increasing Al content (left); phase composition at fixed Al content for different temperatures (right)

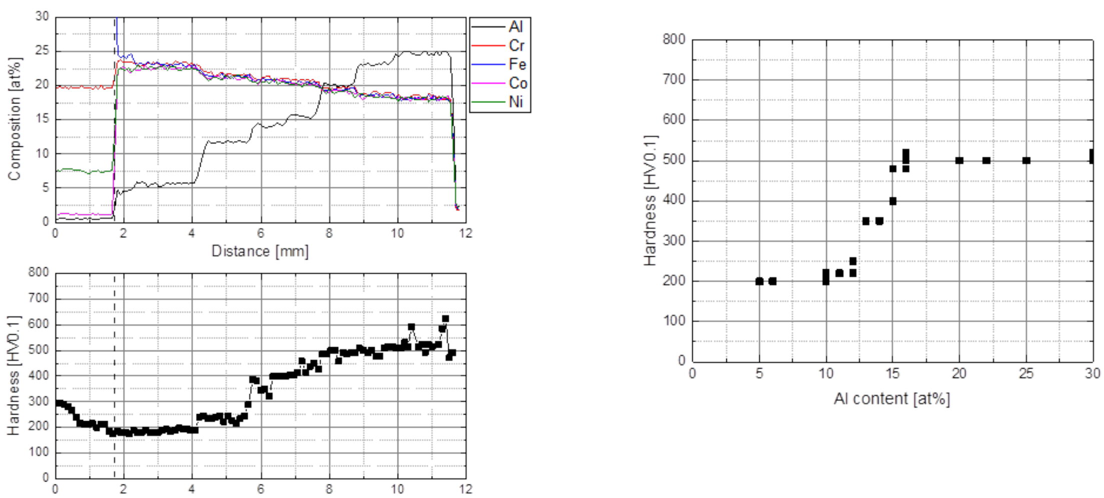

Fig. 3 Chemical composition and hardness of as-built gradient: exemplary designed gradient of 5/15/25 at.% Al (left); hardness as a function of the Al content determined from multiple gradients (right)

dispersive X-ray spectroscopy (EDS) and electron backscatter diffraction (EBSD) in a JEOL JSM-7800F field emission SEM and a JIB-4610F multi beam system. For EDS and EBSD analysis an Oxford X-Max and NordlysNano detector were used as well as the Aztec data acquisition software. Additionally, sample hardness was measured using a load of 0.1 kgf in a LM247 AT Vickers microhardness tester by LECO.

A selection of samples was heat treated after metallographic characterization to further study phase compositions near thermal equilibrium. The homogenization took place for 20 h in Ar atmosphere at about 1350 K followed by cooling in the oven.

Results and discussion

CALPHAD simulation

Calculations of the phase composition at equilibrium were executed using the software program Thermo-Calc on the basis of the TCNi7 database. The simulations were used to estimate interesting compositional areas in the Al$_x$CoCrFeNi system regarding the phase transformation from FCC to BCC as well as for the comparison of the as-built and as-homogenized sample conditions. A non-equilibrium state is expected for the as-built sample caused by high cooling rates characteristic for the laser cladding process.

Fig. 2 shows the results of the CALPHAD simulations. At elevated temperatures (>1350 K) and

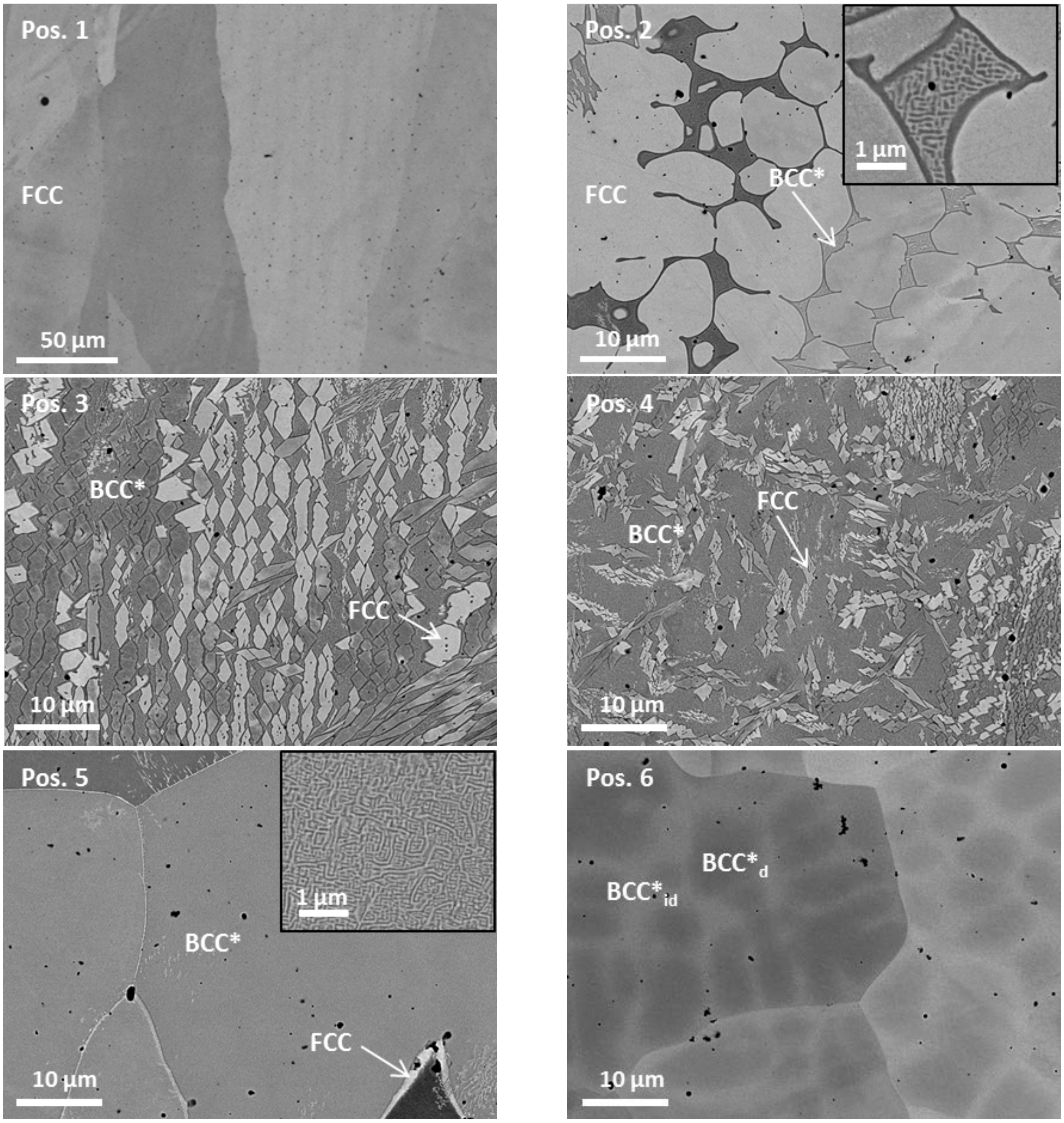

Fig. 4 SEM images of major regions in the as-built gradient: Pos. 1 at 5.0 at.% Al, Pos. 2 at 10.6 at.% Al, Pos. 3 at 13.0 at.%, Pos. 4 at 9.5 at.% Al, Pos. 5 at 14.2 at.% Al, Pos. 6 at 25.8 at.% Al

Al contents below 6 at.% a single phase solid solution FCC microstructure is predicted. In between 6 and 16 at.% Al an additional BCC phase appears (further called BCC1). At 16 at.% a second BCC phase appears (further called BCC2). In between 16 and 20 at.% all three phases (FCC, BCC1 and BCC2) coexist with decreasing amounts of FCC with increasing Al contents. At 20 at.% Al content the microstructure is fully BCC consisting of BCC1 and BCC2.

As-built condition

The chemical composition and hardness of one deposited gradient volume can be seen in Fig. 3. Some deviations from the designed layer compositions (5/15/25 at.% Al) can be observed due to intermixing between the deposited layers. Generally the hardness increases with increasing overall Al content. Up to an Al content of about 10 at.% the hardness remains constant at about 200 HV. In between 10 at.% and 15 at.% Al content the hardness rapidly increases up to about 500 HV. Beyond the hardness stays at a constant level with added Al. The rapid change in hardness correlates

Tab. 2 Representative EDS analysis of major regions of the as-built samples (at.%)

Pos	Area	Al	Cr	Fe	Co	Ni
1	Overall	5.0	20.6	23.8	24.0	26.7
	FCC	5.0	***20.6***	***23.8***	***24.0***	***26.7***
2	Overall	10.6	19.1	21.4	22.8	26.1
	FCC	8.9	***19.0***	***22.9***	***24.3***	***24.8***
	BCC*	***14.1***	22.1	18.0	20.4	25.4
3	Overall	13.0	18.7	21.0	22.2	25.2
	FCC	9.5	***19.2***	***22.7***	***23.3***	***25.3***
	BCC*	***14.4***	20.1	20.0	21.2	24.3
4	Overall	13.4	18.6	20.9	22.0	25.2
	FCC	9.4	***19.3***	***23.0***	***23.0***	***25.2***
	BCC*	***14.2***	20.8	20.1	21.2	23.8
5	Overall	14.2	18.8	20.1	21.8	25.0
	FCC	-	-	-	-	-
	BCC*	***14.2***	18.8	20.1	21.8	25.0
6	Overall	25.8	15.0	16.6	19.9	22.6
	BCC*$_{d}$	***30.3***	10.9	13.6	19.9	***25.3***
	BCC*$_{id}$	20.9	***21.9***	***20.8***	18.9	17.5

with a change in phase composition from single phase FCC to multiphase BCC with increasing Al content, as can be seen in Fig. 4 and Tab. 2. Over the three gradient samples five major microstructures could be observed.

Position 1 displays a single phase FCC solid solution structure with an Al content of about 5.0 at.% and a hardness around 200 HV. At position 2 the overall Al content was increased to 10.6 at.% and a multiphase microstructure can be observed. The microstructure consists of the previously mentioned solid solution FCC phase (now with an Al content of about 8.9 at.%) and interdendritic BCC* with an integrated Al content of about 14.1 at.%. Upon closer examination of the BCC* area a complex multiphase microstructure becomes evident. This is further supported by the EDS maps depicted in Fig. 5 showing that the BCC* area consists of an Al rich and an Al depleted phase. The EBSD analysis identifies both of these phases as BCC phases. Due to limitations of the method further separation between ordered and disordered BCC phases was not possible. These two phases are assumed to be the Al and Ni rich ordered body centered B2 phase (further called BCC1) and the Cr rich solid solution BCC phase (further called BCC2) which, according to literature and the CALPHAD simulations (Fig. 2), can be expected for this particular HEA system [16–19]. At both position 3 and 4, with overall Al contents of 13.0 at.% and 13.4 at.% respectively, a complex microstructure consisting of the before mentioned BCC* and FCC phase can be observed. These two sample positions correlate to the area of rapid

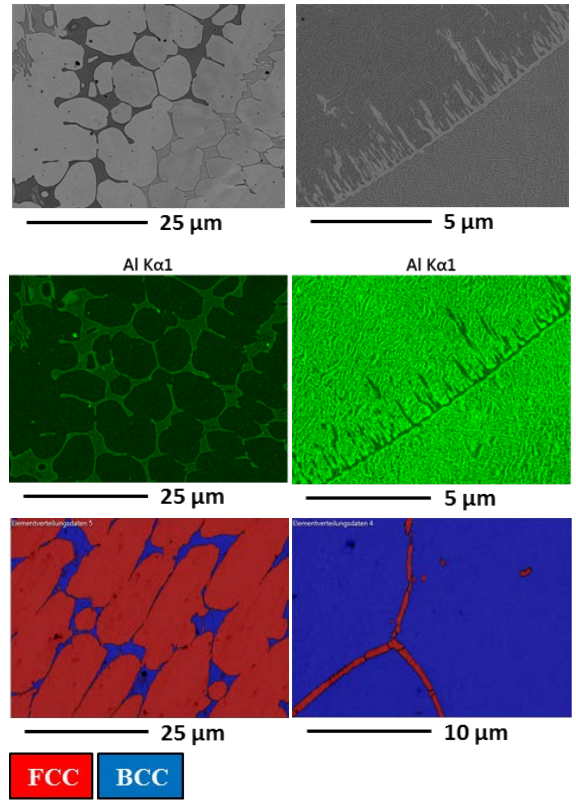

Fig. 5 EDS Al maps and EBSD phase maps of sample positions 2 (left) and 5 (right)

increase in hardness between 10 at.% and 15 at.% Al content. At position 5, with an overall Al content of 14.2 at.%, the microstructure consists mainly of BCC* with residual FCC at the grain boundaries (Fig. 5). At position 6, with an overall Al content of 25.8 at.%, no more residual FCC could be found and the microstructure is entirely BCC*. Additionally the segregation of Al with the formation of Al rich interdendritic regions (BCC*$_{id}$) can be observed. At this position the hardness peaks reach values of about 500 HV.

In comparison to the CALPHAD simulations and the literature [10, 11] the phase composition in relation to the overall Al content of the as-built gradients strongly differs from the described behavior at thermal equilibrium. The transitional area between FCC and multiphase BCC* microstructure according to EDS data and measured hardness lies in between about 10 at.% and 15 at.% Al content (Fig. 3) and is therefore much smaller than the expectations at thermal equilibrium (Fig. 2). Additionally the BCC* multiphase structure can be observed as early as the first occurrence of BCC phase at position 2 in contrast to the expected stepwise occurrence of first BCC1 and then BCC2. It is known, that the

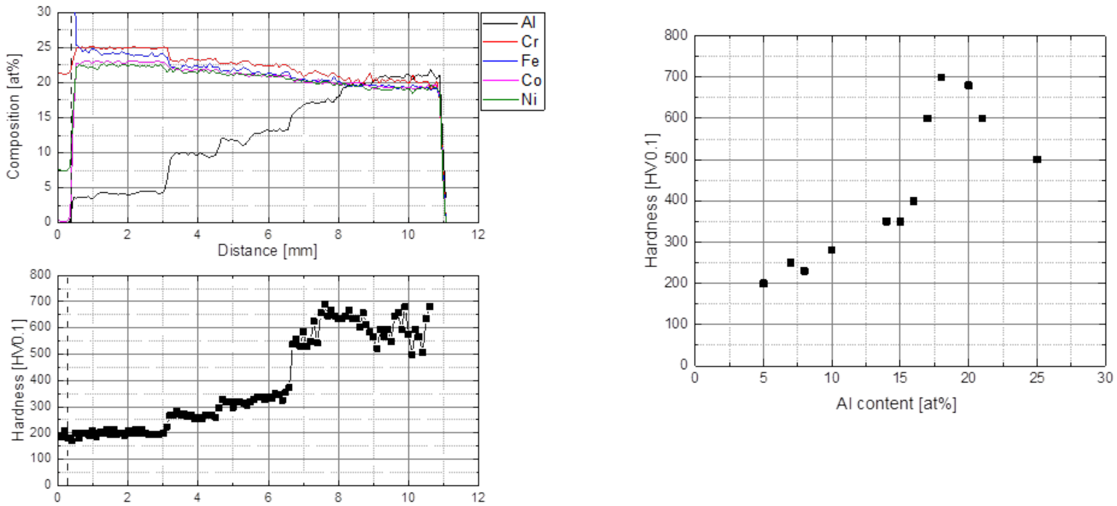

Fig. 6 Chemical composition and hardness of as-homogenized gradients; as-homogenized designed gradient of 5/15/15 at.% Al (left); hardness as a function of the Al content determined from multiple gradients (right)

Tab. 3 Representative EDS analysis of major regions of the as-homogenized samples (at.%)

Pos	Area	Al	Cr	Fe	Co	Ni
1	Overall	4.8	24.3	23.8	23.8	23.3
	FCC	4.8	***24.3***	***23.8***	***23.8***	***23.3***
2	Overall	10.4	22.4	22.2	22.5	22.5
	FCC	5.9	***25.6***	***24.6***	***23.8***	20.1
	BCC1	***29.1***	7.5	11.6	17.1	***34.7***
3	Overall	14.7	21.2	21.1	21.4	21.6
	FCC	5.7	***27.8***	***27***	***23.3***	16.1
	BCC1	***28.2***	10.2	13.0	18.6	***30.1***
4	Overall	17.5	20.6	20.2	20.6	21.1
	FCC	5.3	***27.3***	***28.7***	***24.1***	14.6
	BCC1	***27.7***	9.0	13.8	20.0	***29.6***
	BCC2	3.4	***44.2***	***27.5***	18.7	6.2
5	Overall	23.5	18.0	18.4	19.8	20.3
	BCC1	***28.8***	10.6	15.2	20.8	***24.7***
	BCC2	4.0	***46.2***	***30.4***	15.1	4.3
6	Overall	24.6	19.5	18.8	18.8	18.3
	BCC1	***28.4***	14.2	16.5	19.8	***21.1***
	BCC2	7.6	***47.7***	***31.8***	10.0	2.9

extremely rapid solidification typical of laser cladding leads to non-equilibrium structures having slightly different compositions/properties from the bulk. This effect can be compensated by applying a heat treatment.

As-homogenized condition

Fig. 6 shows the chemical composition and hardness of the as-homogenized gradient sample. The sample shows some deviations from the designed layer compositions due to intermixing between the deposited layers. Up to an Al content of about 5 at.% hardness stays at about 200 HV. In between 5 at.% and 18 at.% overall Al content hardness steadily increases from about 200 HV up to about 700 HV. Eventually hardness drops down to about 500 HV at 25 at.% overall Al content.

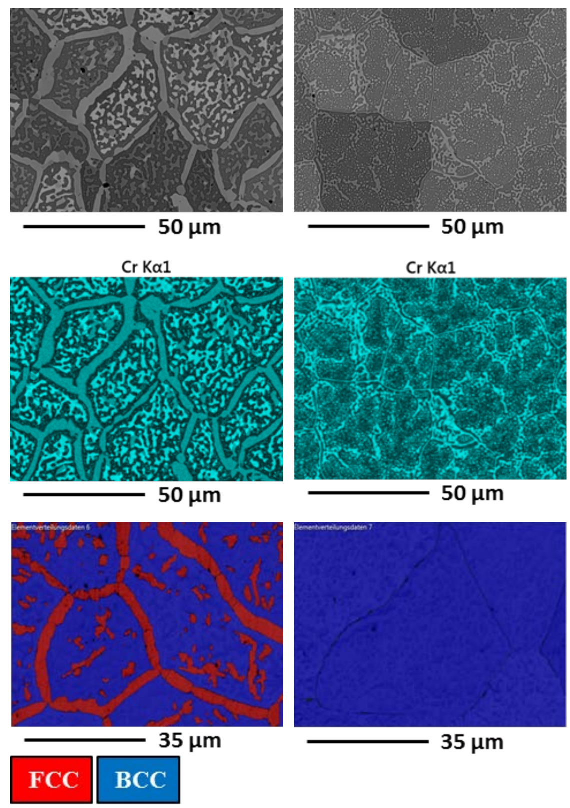

Fig. 7 EDS Cr maps and EBSD phase maps of sample positions 4 (left) and 6 (right)

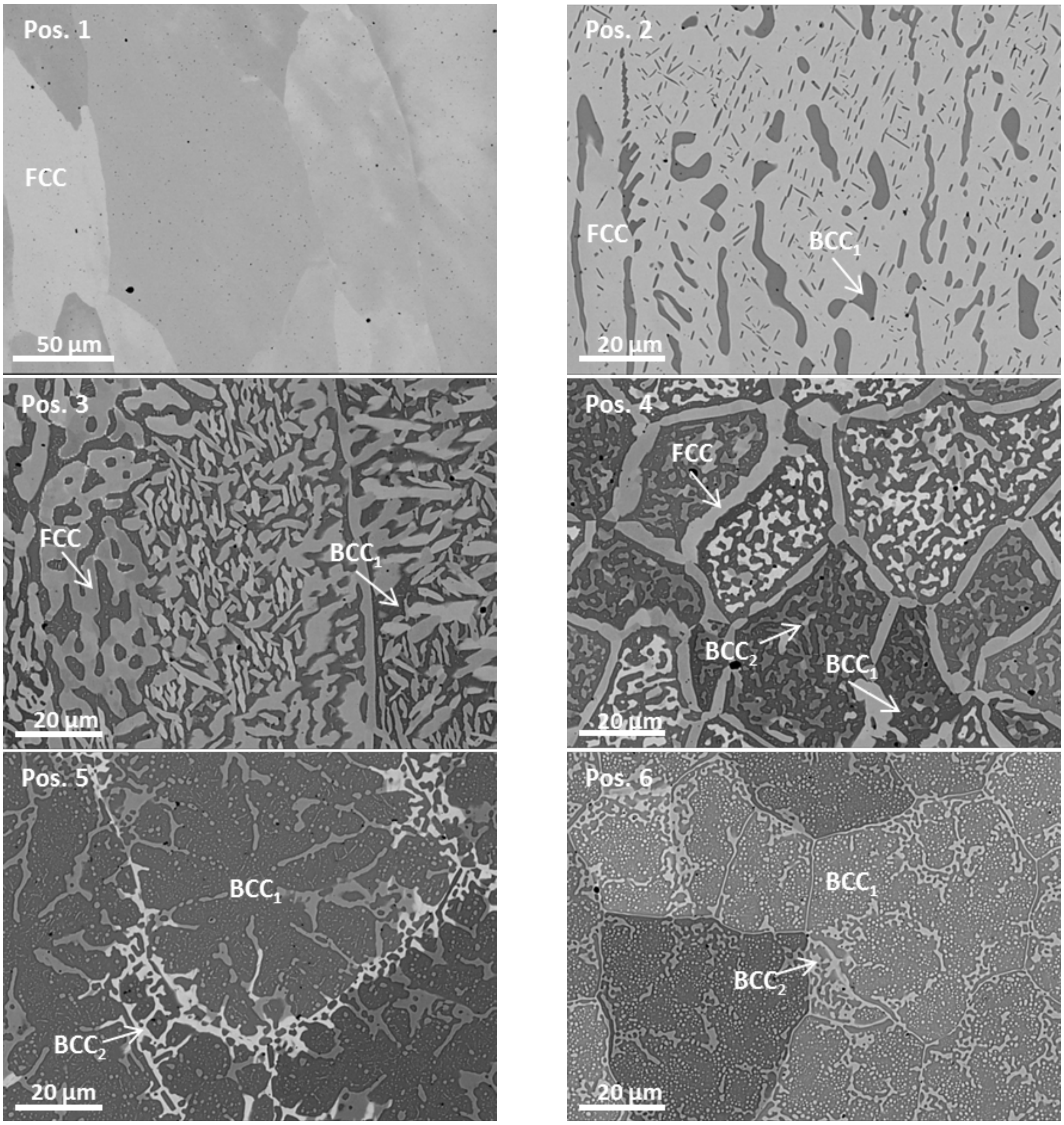

Fig. 8 SEM images of major regions in the as-homogenized gradient: Pos. 1 at 4.8 at.% Al, Pos. 2 at 10.4 at.% Al, Pos. 3 at 14.7 at.% Al, Pos. 4 at 17.5 at.% Al, Pos. 5 at 23.5 at.% Al, Pos. 6 at 24.6 at.% Al

The change in hardness again correlates with a change in microstructure with added Al as can be seen in Fig. 8 and Tab. 3. Over the three samples four major microstructures could be observed.

Position 1 displays a solid solution FCC structure with an overall Al content of 4.8 at.%. At position 2, with an overall Al content of 10.4 at.%, an additional Al and Ni rich phase appears. In accordance to the literature [16–19] and CALPHAD simulations this phase is assumed to be the disordered body centered B2 phase (BCC1). At position 3, with an overall Al content of 14.7 at.%, the amount of BCC1 steadily increases correlating to the increase of hardness from about 200 HV towards about 350 HV. At position 4, with an overall Al content of 17.5 at.%, a complex multi phased microstructure can be observed. As depicted in the EBSD and EDS maps in Fig. 7 this complex microstructure consists of the Al depleted FCC grain boundary phase, the Al and Ni rich BCC1 phase and a Cr and Fe rich solid solution BCC phase (BCC2) [16–19]. Again the distinction between solid solution BCC and ordered body centered B2 phase was not possible using EBSD. For this position the highest value of hardness (about 700 HV) was measured. At positions 5 and 6, with Al contents of 23.5 at.% and 24.6 at.%, respectively, the microstructure is fully BCC with a decreasing amount of BCC2 at higher Al contents. The hardness of these positions was about 500 HV.

According to the change in sample hardness and the EDS analysis the transitional area between solid solution FCC and multiphase BCC microstructure for the as-homogenized samples lies in between 5 at.% and 23 at.% Al content. The first observed BCC phase is the Al and Ni rich BCC1 phase followed by the Fe and Cr rich BCC2 phase at about 17 at.% Al content. This fits well into the CALPHAD data as well as into similar findings in literature [10, 11]. At about 17 at.% Al content the hardness reaches values as high as 700 HV which might be contributed to the Hall Petch relationship.

Conclusions

In this manuscript, microstructures and mechanical properties of $Al_xCoCrFeNi$ HEA prepared by means of laser cladding were investigated in detail. Applying a nozzle with four evenly distributed powder inlets allowed an effective microstructural screening by designing a gradient structure within a single-step process. The main findings of the present study can be resumed as follows:

(1.) In the as-built as well as in the as-homogenized condition hardness increases with increasing Al content.

(2.) In the as-built sample condition, between 10 at.% and 15 at.% Al content, the microstructure changes from solid solution FCC to multiphase BCC (B2 and solid solution BCC). Simultaneously the hardness increases from 200 HV to 500 HV.

(3.) The transformation behavior of the as-built samples differs from the CALPHAD simulation at thermal equilibrium. This is due to the non-equilibrium state of the laser cladding structure, resulting from the high cooling rates.

(4.) In the as-homogenized sample condition, in between 5 at.% and 23 at.% Al content, the microstructure changes from solid solution FCC towards multiphase BCC (B2 and solid solution BCC) and simultaneously the hardness increases from 200 HV at 5 at.% Al content towards 700 HV at 17 at.% Al content and then decreases towards 500 HV at 23 at.% Al content.

(5.) The transformation behavior of the as-homogenized samples well into the CALPHAD simulations at thermal equilibrium.

The laser cladding process is excellently appropriate for the development of new HEA systems. During welding, the composition of the HEA layer was specifically varied within a single process step. The Fraunhofer IWS coaxial ring nozzle and the parallel connection of several powder feeders allows the composition of the HEA to be varied with each deposited layer. $Al_xCoCrFeNi$ coatings could be manufactured reliably, demonstrating high chemical and structural homogeneity without macroscopic segregations and only minor amounts of impurities**.**

References

[1] M. C. Gao, J.-W. Yeh, P. K. Liaw, and Y. Zhang, Eds., *High Entropy Alloys: Fundamentals and Applications*: Springer, 2016.

[2] S. Gorsse, D. B. Miracle, and O. N. Senkov, “Mapping the world of complex concentrated alloys,” *Acta Materialia*, vol. 135, pp. 177–187, 2017.

[3] S. John Mary, R. Nagalakshmi, and R. Epshiba, “High entropy alloys properties and its applications - an overview,” *Eur. Chem. Bull*, vol. 4, no. 6, pp. 279–284, 2015.

[4] D. B. Miracle and O. N. Senkov, “A critical review of high entropy alloys and related concepts,” *Acta Materialia*, no. 122, pp. 448–511, 2017.

[5] M.-H. Tsai and J.-W. Yeh, “High-Entropy Alloys: A Critical Review,” *Materials Research Letters*, vol. 2, no. 3, pp. 107–123, 2014.

[6] B. Cantor, I. Chang, P. Knight, and A. Vincent, “Microstructural development in equiatomic multicomponent alloys,” *Materials Science and Engineering A*, vol. 375-377, pp. 213–218, 2004.

[7] Z. Tang *et al.*, “Tensile ductility of an AlCoCrFeNi multi-phase high-entropy alloy through hot isostatic pressing (HIP) and homogenization,” *Materials Science & Engineering A*, no. 647, pp. 229–240, 2015.

[8] K. Kuwabara *et al.*, “Mechanical and corrosion properties of AlCoCrFeNi high-entropy alloy fabricated with selective electron beam melting,” *Additive Manufacturing*, vol. 23, pp. 264–271, 2018.

[9] D. Karlsson *et al.*, “Binder jetting of the AlCoCrFeNi alloy,” *Additive Manufacturing*, vol. 27, pp. 72–79, 2019.

[10] Y.-F. Kao, T.-J. Chen, S.-K. Chen, and J.-W. Yeh, “Microstructure and mechanical property of as-cast, -homogenized, and -deformed AlxCoCrFeNi ($0 \leq x \leq 2$) high-entropy alloys,” *Journal of Alloys and Compounds*, vol. 488, pp. 57–64, 2009.

[11] H.-P. Chou, Y.-S. Chang, S.-K. Chen, and J.-W. Yeh, “Microstructure, thermophysical and electrical properties in AlxCoCrFeNi (0≤x≤2) high-entropy alloys,” *Materials Science and Engineering: B*, vol. 163, pp. 184–189, 2009.
[12] F. Brückner *et al.*, “Process characteristics in high-precision laser metal deposition using wire and powder,” *Journal of laser applications*, vol. 29, 2017.
[13] F. Brueckner *et al.*, “Enhanced manufacturing possibilities using multi-materials in laser metal deposition,” *Journal of laser applications*, vol. 30, no. 3, pp. 1–8, 2018.
[14] S. Chen, Y. Tong, and P. Liaw, “Additive Manufacturing of High-Entropy Alloys: A Review,” *entropy*, vol. 937, no. 20, pp. 1–18, 2018.
[15] W. E. Frazier, “Metal Additive Manufacturing: A Review,” *Journal of Materials Engineering and Performance*, vol. 23, 2014.
[16] Hiroshi Shiratori *et al.*, “Relationship between the microstructure and mechanical properties of an equiatomic AlCoCrFeNi high-entropy alloy fabricated by selective electron beam melting,” *Materials Science & Engineering A*, vol. 656, 201.
[17] D. Karlsson *et al.*, “Elemental segregation in an AlCoCrFeNi high-entropy alloy – A comparison between selective laser melting and induction melting,” *Journal of Alloys and Compounds*, vol. 784, pp. 195–203, 2019.
[18] I. Kunce, M. Polanski, K. Karczewski, T. Plocinski, and K. J. Kurzydlowski, “Microstructural characterisation of high-entropy alloy AlCoCrFeNi fabricated by laser engineered net shaping,” *Journal of Alloys and Compounds*, vol. 648, pp. 751–758, 2015.
[19] C. Zhang *et al.*, “Understanding phase stability of Al-Co-Cr-Fe-Ni high entropy alloys,” *Materials and Design*, vol. 109, pp. 425–433, 2016.

Meet the Authors

Martin Kuczyk graduated at the Technical University of Chemnitz in the field of Physics. He is now working in the division Materials Characterization and Testing at the Fraunhofer IWS in Dresden with a special focus on electron microscopic material and failure analysis.

Liliana Kotte studied material science at the Technical University of Dresden. She finished her PhD in theoretical and practical aspects of atmospheric pressure plasma technology for surface modification. After focusing on CVD technologies, she works in the group thermal surface technology at Fraunhofer IWS since 2017. Her work mainly focuses on material development generated with nozzle-based laser cladding processes.

Jörg Kaspar holds a PhD in Physics from the Technical University of Dresden and is leading the group of material and failure analysis at the Fraunhofer IWS since 2010. He is a dedicated expert in high resolution imaging and analysis by means of electron microscopy focusing on the exploration of process-structure-property correlations of complex materials and composites.

Maria Barbosa holds a PhD in Materials Engineering from the Technical University of Dresden and has been working with thermal spray and laser cladding coatings at Fraunhofer IWS for the last 10 years. She is the group manager of the thermal spray unit and the deputy manager of the thermal coating department, where together with her team they explore different technologies to find the perfect coating solution.

Prof. Steffen Nowotny finished his PhD work in 1987 and now manages the business unit thermal surface technology at Fraunhofer IWS. He is responsible for applied RD projects in laser surface cladding and system technology as well as the supervision of industrial users. Also, he has a lectureship on Generative Manufacturing at the Technische Universitaet Dresden.

Prof. Martina Zimmermann studied mechanical engineering and earned her PhD in 2001 at the University of Siegen. Since 2012 she owns a professorship at the Technical University of Dresden in Mechanics of Materials and Failure Analysis. Simultaneously she is leader of the department Material Characterization and Testing at the Fraunhofer IWS. Her research focusses on the identification of microstructure and deformation behaviour to assess component reliability.

Born in 1967, **Prof. Christoph Leyens** studied physical metallurgy and materials technology at RWTH Aachen, Germany, where he earned his diploma in 1993 and his Ph.D. in 1997. He is currently a full professor for materials science and engineering at the Technical University of Dresden, Germany, and director of the Fraunhofer IWS, Dresden. Leyens has covered a wide range of research topics with a focus on high temperature and lightweight materials, surface technology and additive manufacturing. He has published more than 200 papers, seven books and holds eleven patents.